Conference Paper, Published Version

Gourgue, Olivier; Sishah, Biniyam; Vanlede, Joris; Komijani, Homayoon; Chen, Margaret

Modelling tides and storm surges on the European continental shelf

Modelling tides and storm surges on the European continental shelf

Olivier Gourgue[1,2], Biniyam B. Sishah[1], Joris Vanlede[2], Homayoon Komijani[3] & Margaret Chen[1]
[1] Department of Hydrology and Hydraulic Engineering, Vrije Universiteit Brussel, Brussels, Belgium
[2] Flanders Hydraulics Research, Flemish Government, Antwerp, Belgium
[3] Hydraulics Section, Katholieke Universiteit Leuven, Leuven, Belgium
ogourgue@gmail.com

***Abstract*—This paper presents an effort to simulate the propagation of tides and storm surges through the Northwestern European continental shelf using a slightly modified version of TELEMAC-2D v7p0r1. The area of interest is the Belgian Continental Shelf and the model is calibrated accordingly.**

I. INTRODUTION

A storm surge is an offshore rise of water, which is primarily caused by winds pushing on the sea surface. In shallow water areas, storm surges can be particularly damaging when they occur at the time of a high tide, potentially causing devastating coastal flooding. This phenomenon is one of the major natural threats for the Belgian coastal area and the region surrounding the tidal part of the Scheldt basin. It is therefore a subject of high interest in terms of long-term coastal protection and sustainable development in Belgium.

Studying local impacts of storm surges is a rather multi-scale problem as the latter are formed at the scale of the entire North Sea. The use of an unstructured grid model seems therefore to be a natural choice, thanks to their ability to simulate various scale processes in a rather flexible way.

Storm surges are especially damaging when occurring during a very high tide. It is therefore essential to represent accurately the tides when evaluating the impact of storm surges. In a first step, the present paper focuses on the set up of a tidal model (no influence of wind, nor waves) based on TELEMAC-2D and its calibration for best representation of tides in the area of interest. The influence of meteorological conditions (wind velocity and air pressure) to form storm surges is discussed in a second step.

II. MATERIALS AND METHODS

A. Grids

Two grid configurations are considered in this study, both covering the entire Northwestern European continental shelf. In the first configuration (Fig. 1), the open boundary offshore is located at the shelf break, which is defined as the 200 m isobath. This strategy already proved its efficiency to simulate the tides in Belgian and Dutch coastal waters with the finite element model SLIM [1]. In the second configuration (Fig. 2), the computational domain is extended to deeper parts in the Atlantic Ocean, so that the formation and propagation of very long waves can be simulated explicitly without nesting with a larger scale model or resorting to external data.

The coastlines are generated using the PUG[1] Matlab toolbox and the grids are generated using the open source application Gmsh [2,3]. In both configurations, the mesh density varies as a function of

1. the distance to the coastlines (the mesh density increases when getting closer to the coastlines, to have a good representation of them without increasing the computer cost offshore), and
2. the distance to the area of interest (the mesh density increases when getting closer to the Belgian coast and the Scheldt estuary).

B. Model setup

TELEMAC-2D v7p0r1 is used in this study, but it is slightly modified so that

1. the Coriolis parameter is evaluated as a function of the latitude, even on a Cartesian grid,
2. the tidal force is taken into account in the momentum equation, even on a Cartesian grid,
3. the wind velocity and the air pressure vary in space and time and are extracted from NetCDF files, and
4. the wind drag coefficient is a function of the wind velocity and is parameterized using Flather's formulation [4]:

$$c_d = \begin{cases} 0.565 \cdot 10^{-3} & \text{if } \|\boldsymbol{w}\| \leq 5\,, \\ (-0.12 + 0.137\|\boldsymbol{w}\|) \cdot 10^{-3} & \text{if } 5 \leq \|\boldsymbol{w}\| \leq 19.22\,, \\ 2.513 \cdot 10^{-3} & \text{if } \|\boldsymbol{w}\| \geq 19.22\,, \end{cases}$$

where $\boldsymbol{w}$ is the wind velocity vector 10 m above the water surface and is expressed in m/s in the above equation.

Manning's formulation is chosen to parameterize the bottom friction. A constant viscosity of 10^{-6} m^2/s is chosen for the turbulence model, assuming that the numerical diffusion of the model is sufficient to account for subgrid scale phenomena. The generalized wave continuity equation reformulation is

[1] http://www.oliviergourgue.net/pug

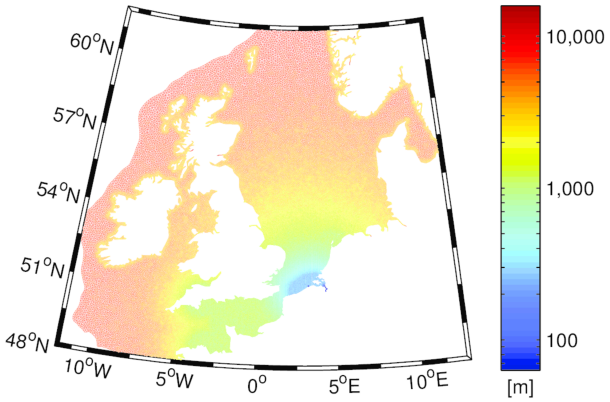

Figure 1: First grid configuration with the offshore boundary at the shelf break; the grid is made up with 320223 triangles sharing 156345 nodes; the colour scale represents the characteristic length of the triangles, ranging from 100 m in very detailed parts of the area of interest to 15 km offshore; the resolution is about 200 m in the Belgian Continental Shelf.

used to solve the primitive shallow water equations. Linear and quasi-bubble approximations are used to discretize the water depth and the horizontal depth-averaged velocity, respectively. Time integration is fully implicit and the time step is 60 s.

C. *Forcing data*

1) Bathymetry: Different datasets are used to describe the bathymetry of the computational domain. The main properties of the different datasets are summarized in Table 1. They are listed by decreasing order of importance. For a given dataset, all the data located inside the area of another dataset of higher importance are excluded from the final aggregated dataset. The latter is used to interpolate the bathymetry on the unstructured grid nodes.

Table 1: List of the different bathymetry datasets and their main properties, by order of importance.

	Covered area	*Spatial resolution*	*Measurement period*	*Source*
1	Belgian Continental Shelf	1-200 m	2007-2010	MDK Afdeling Kust
2	Western Scheldt	20 m	2011	Rijkswaterstaat
3	Lower Sea Scheldt	1 m	2012	Vlaamse Milieu-maatschappij
4	European seas and oceans	0.125 arc-minute	February 2015[2]	EMODnet

2) Tides in the deep ocean: The tides are the main forcing mechanism of the system. They are imposed at the offshore

[2] Date of release.

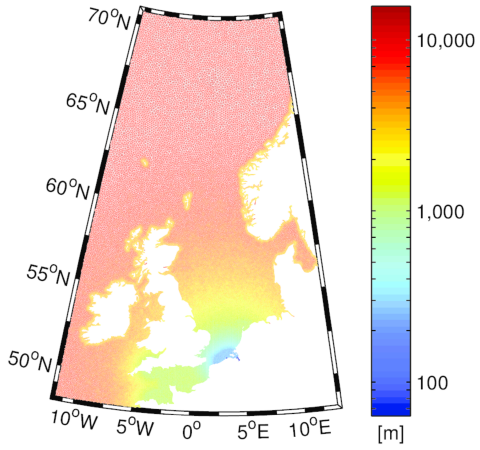

Figure 2: Second grid configuration with the offshore boundary in the Atlantic Ocean (along the 48°N, 12°W, 71°N and 13°E lines); the grid is made up with 341802 triangles sharing 166728 nodes; the colour scale represents the characteristic length of the triangles, ranging from 100 m in very detailed parts of the area of interest to 15 km offshore; the resolution is about 200 m in the Belgian Continental Shelf.

boundary of the domain using OSU Tidal Data Inversion products [5,6]. In the case of the open boundary at the shelf break (Fig. 1), the OTIS Atlantic Ocean tidal solution is used. It provides the amplitude and phase of 11 harmonic constituents over the Atlantic Ocean with a resolution of 5 arc-minutes. However, this dataset does not cover entirely the computational domain of the second configuration (Fig. 2). In that case, the OSU TOPEX/Poseidon Global Inverse Solution TPXO is used. It provides the amplitude and phase of 13 harmonic constituents over the global ocean, but with a resolution of 15 arc-minutes. The tidal signal at the offshore boundary of the domain is reconstructed by TELEMAC from these datasets, and it simply propagates through the domain, slightly nourished by the tidal force.

3) Atmospheric fields: The meteorological conditions contribute less to the movement of water masses in the region. However, the wind and the air pressure are the key factors responsible for the generation of storm surges, which can be particularly damaging when they occur at the time of a high tide, potentially causing devastating coastal flooding. In this study, the horizontal wind velocity vector 10 m above the mean sea level and the air pressure at the water surface are in used. They are extracted from the ERA-Interim global atmospheric reanalysis produced by the European Centre for Medium-Range Weather Forecasts (ECMWF), which covers the period from 1979 onwards, with a spatial resolution of 7.5 arc-minutes and a frequency of 6 hours [7].

D. *Simulated periods*

This study is carried out in the framework of a larger project, whose objective is to study wind waves and surge levels in the Belgian Continental Shelf during super storms, with a focus on the important storm surge event that affected the coastal margins of the southern North Sea on 5-6 December 2013 [8], as a consequence of the Cyclone Xavier, also known

ad the *Sinterklaasstorm* in Flanders and the Netherlands. For this reason, 2013 is selected as the target year for the entire project.

However, when focusing on tides, it is important to select a calm period in terms of meteorological conditions, in order to limit the influence of wind waves and surge levels on the measurements. In that case, the model is run over July 2013, as it is the month with the weakest winds in the Belgian Continental Shelf that year. On the other hand, December 2013 is selected when the influence of strong wind events is investigated. In both cases, a spin up period of 5 days is run before, to make sure that all transients effects associated with the initialization are dissipated.

E. Performance indicators

Different statistics are used to estimate the model performance. The correlation coefficient R is used to quantify pattern similarity between model results f and observations r, and is defined as

$$R = \frac{\frac{1}{N}\sum_{i=1}^{N}(f_i - \bar{f})(r_i - \bar{r})}{\sigma_f \sigma_r},$$

where f_i and r_i are the discrete values at N different times of f and r, respectively, $\bar{f}$ and $\bar{r}$ their mean values, and σ_f and σ_r their standard deviations, with

$$\bar{x} = \frac{1}{N}\sum_{i=1}^{N} x_i ,$$

$$\sigma_x = \sqrt{\frac{1}{N}\sum_{i=1}^{N}(x_i - \bar{x})^2} ,$$

where x must be replaced by either f or r. The correlation coefficient reaches a maximum value of 1 for perfectly correlated variables, i.e. when, for all i, $(f_i - \bar{f}) = \alpha(r_I - \bar{r})$, where α is a positive constant. In that case, the variables have the same centered pattern of variation, but they are not identical unless $\alpha = 1$. The correlation coefficient does not give any information about the similarity in terms of amplitude of variation [9].

The root mean square (RMS) error E is used to quantify the differences between model results and observations, and is defined as

$$E = \sqrt{\frac{1}{N}\sum_{i=1}^{N}(f_i - r_i)^2} .$$

In order to isolate the differences in the patterns from the differences in the means, the RMS error is split into the overall bias

$$\bar{E} = \bar{f} - \bar{r} ,$$

and the centered pattern RMS error

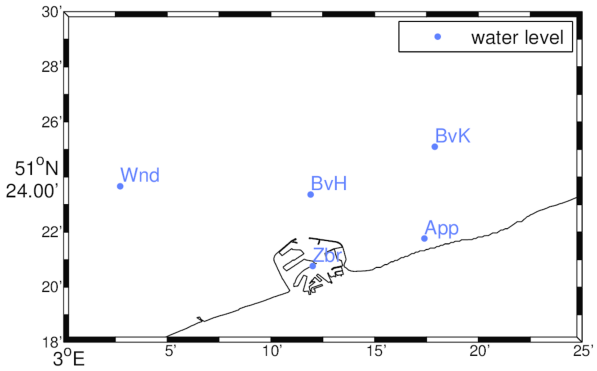

Figure 3: Flemish Banks Monitoring Network stations where observation data have been collected; the official station names are given in Table 2.

$$E' = \sqrt{\frac{1}{N}\sum_{i=1}^{N}\left((f_i - \bar{f}) - (r_i - \bar{r})\right)^2} ,$$

which tends to zero when two patterns become alike, but does not determine how much of the error is due to the structure and phase and how much is due to a difference in the amplitude of the variations [9].

The correlation coefficient and the RMS errors provide complementary statistical information about the model performance, but they must be associated with the standard deviations to include information about amplitude of pattern variation. To facilitate the analysis, those indicators are displayed in a Taylor diagram [9], as for example on the top panel of Fig. 4. In such diagram:

1. the set of observations at one location and the model results at the same location are all represented by single dots (in red in this paper),
2. the standard deviation of a given pattern is the distance between the corresponding dot and the origin (in black)
3. the centered pattern RMS error of a given simulation is the distance between the corresponding simulation dot and the observation dot (in green), and
4. the correlation coefficient between the model results of a given simulation and the observations is given by the azimuthal angle of the corresponding simulation dot (in blue).

F. Measurement stations

The observation data used to evaluate the model performance have been collected in the framework of the Flemish Banks Monitoring Network[3], which is made up of measuring pillars, wave data buoys and hydro-meteo sensors in the Belgian Continental Shelf. The measurements stations whose data are used in this study are displayed on Fig. 3 and their coordinates are given in Table 2.

[3] *Meetnet Vlaamse Banken* – http://www.meetnetvlaamsebanken.be

Table 2: Coordinates of the Flemish Banks Monitoring Network stations where observation data have been collected.

Abbreviation	*Official name*	*Latitude*	*Longitude*
App	Appelzak	51°21'46"N	3°17'24"E
BvH	Bol van Heist	51°23'22"N	3°11'55"E
BvK	Bol van Knokke[4]	51°25'6"N	3°17'54"E
Wan	Wandelaar	51°23'40"N	3°2'44"E

III. Results and Discussion

A. Influence of the offshore boundary location

As mentioned previously, two configurations are considered for the location of the offshore open boundary. In the first one, the offshore boundary is located at the shelf break (Fig. 1). In the second one, the computational domain is extended further in the Atlantic Ocean (Fig. 2). The first configuration already proved appropriate to simulate the tidal dynamics in the area of interest [1]. The second configuration could be interesting to simulate explicitly the formation of wind waves and storm surges in deep areas, together with their propagation towards the continental shore, using a single multi-scale model. The first objective of this paper is to verify that the quality of the tidal simulations is not altered when extending the computational domain. To do so, the model is roughly calibrated over July 2013 using different values of the Manning coefficient, in both grid configurations. The influence of the meteorology is not taken into account here (see simulations S1a to S2f in Table 3).

Taylor diagrams of the water elevation at Wandelaar for simulation sets S1 and S2 are displayed on the top panels of Figs. 4 and 5, respectively. The results at the other stations are very similar and are therefore not shown. Those diagrams show that the Manning coefficient has a clear effect on the standard deviation of the water surface elevation. This is due to the damping role that bottom friction has on tides: the higher the bottom friction, the lower the amplitude of the tidal variation. Also, using the second grid configuration (extended domain) instead of the first one (offshore boundary at the shelf break) seems to move the simulation dots towards the right, i.e. towards higher standard deviations of the water level. As a consequence, the optimal value of the Manning coefficient is not the same for both configurations. It is $0.022 s/m^{1/3}$ for the offshore boundary at the shelf break (simulation S1b), and $0.024 s/m^{1/3}$ in the case of the extended domain (simulation S2c).

[4] Also know as Scheur Wielingen.

Table 3: Main parameters for each simulation.

	Grid configuration	*Manning coefficient* $[s/m^{1/3}]$	*Tidal forcing shift [m]*	*Meteo*	*Period*
S1a	Shelf break (Fig. 1)	0.020	No	No	Jul. 2013
S1b		0.022			
S1c		0.024			
S1d		0.026			
S1e		0.028			
S1f		0.030			
S2a	Extended (Fig. 2)	0.020			
S2b		0.022			
S2c		0.024			
S2d		0.026			
S2e		0.028			
S2f		0.030			
S3a		0.024	-0.05		
S3b			-0.10		
S3c			-0.15		
S4			-0.10	Yes	
S5a				No	Dec. 2013
S5b				Yes	

B. Influence of the mean sea level at the open boundary

When compared to observations, the results of simulation S2c present a negative bias of the order of 0.1 m. One explanation could be that the bathymetry is defined with respect to the vertical datum NAP (*Normaal Amsterdams Peil*, or Amsterdam Ordnance Datum) while the tidal boundary conditions are defined with respect to the ocean mean sea level, which could be slightly different.

In order to neutralize this bias, a uniform vertical shift is applied at the open boundary to the mean sea level, around which the water elevation tidal forcing oscillates. A set of three simulations is run with different values of this tidal forcing shift. The rest of the setup is the same as the best extended grid simulation S2c (see Table 3). The evolution of the bias at the different measurement stations is presented on Fig. 6. The best model results are obtained with a tidal forcing shift of -0.1 m (simulation S3b), but the optimal value seems to be somewhere between -0.15 and -0.1 m.

C. Influence of the meteorological conditions

Simulation S4 is run to investigate the influence of meteorological conditions during calm weather. The setup is

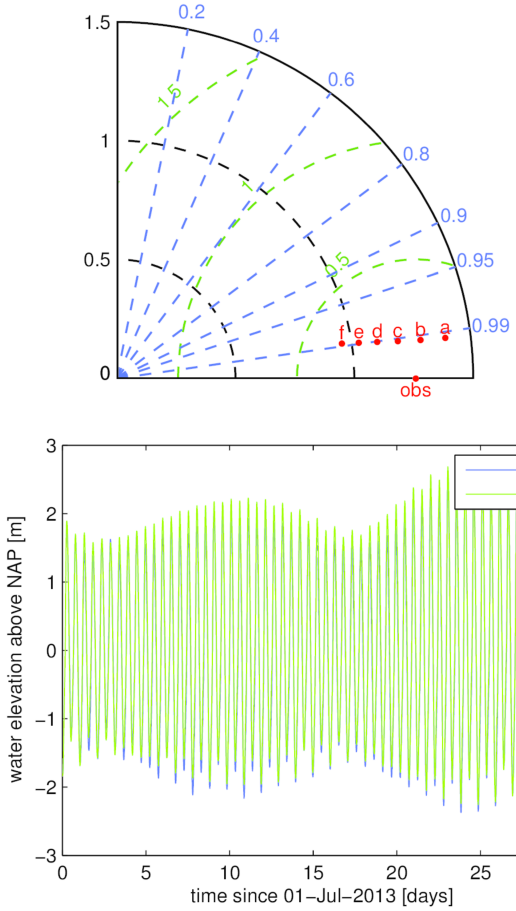

Figure 4: [Upper panel] Taylor diagram comparing water elevation from simulations S1a to S1f with observations at Wandelaar; standard deviations σ_f and σ_r are given in black, correlation coefficient R in blue, and centered pattern RMS error E' in green. [Bottom panel] Water elevation time series at Wandelaar from simulation S1b and observations.

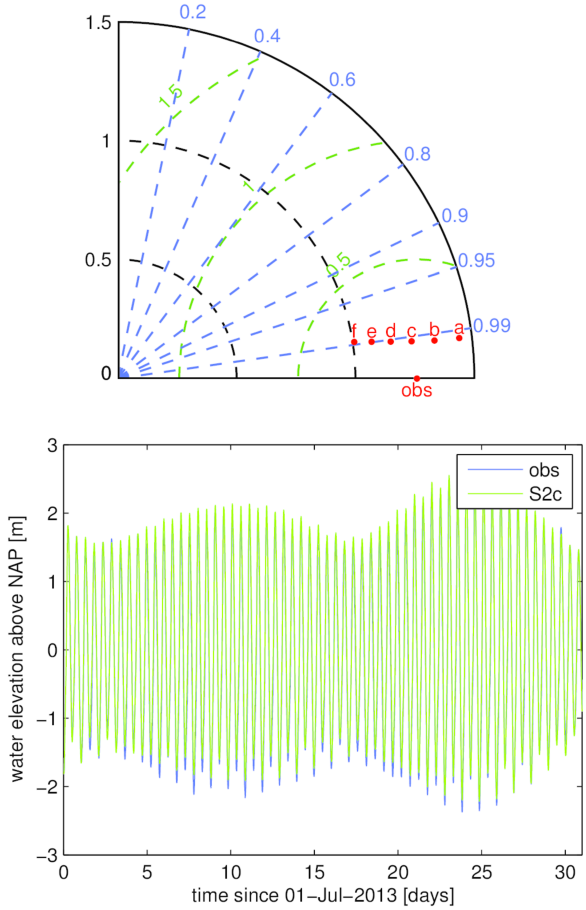

Figure 5: [Upper panel] Taylor diagram comparing water elevation from simulations S2a to S2f with observations at Wandelaar; standard deviations σ_f and σ_r are given in black, correlation coefficient R in blue, and centered pattern RMS error E' in green. [Bottom panel] Water elevation time series at Wandelaar from simulation S2c and observations.

the same as simulation S3b, except that the wind and the air pressure are now taken into account (see Table 3).

The differences between the two simulations in terms of correlation coefficient, standard deviation and centered pattern RMS error are so small that they cannot be seen on a Taylor diagram: for each station, the simulation dots cannot be distinguished (not shown). On the other hand, taking the atmospheric fields into account influences slightly the bias (Fig. 7), even though the impact is much smaller than applying a tidal forcing shift of the order of 0.1 m (Fig. 6).

Simulations S5a and S5b use the same setups as simulations S3b and S4, respectively, except that they run over December 2013 (see Table 3). Obviously, the influence of the meteorological conditions is much more important during such a windy period, as can be observed on the Taylor diagram on the top of Fig. 8. Both the correlation coefficient and the centered pattern RMS error are significantly improved when including the influence of wind and air pressure in the model. On the other hand, the standard deviation is barely influenced by the meteorological conditions. The vertical oscillations of the water surface are indeed mainly due to tides.

The time series on the bottom panel of Fig. 8 even show that the model is quite good at representing the storm surge of December 5-6 [8]. However, it also seems to overestimate slightly the water surface elevation during the first half of the month, while underestimating it during the second half, especially around December 25. The model behaviour could probably be significantly improved by using a more elaborated parameterization of the wind drag coefficient or by coupling it with a wind wave model, which is the objective of a second phase of the project. Finally, it is worth mentioning that even though Fig. 8 only presents results and observations at Wandelaar, they are very similar at the other stations, so that the above discussion about the influence of the meteorological conditions during a windy period can be assumed to stand for the entire area of interest.

IV. Conclusion

This paper presents the setup of a slightly modified version of TELEMAC-2D v7p0r1 to simulate the propagation of tides and storm surges on the Northwestern European continental shelf, as well as their influence in the Belgian coastal area.

Two grid configurations are considered. In the first one, the open boundary is located on the shelf break, which is a natural

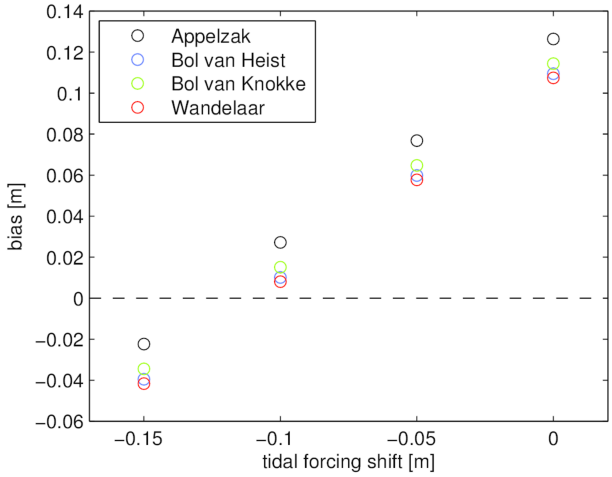

Figure 6: Evolution of the bias at the measurement stations of Fig. 3 for different values of the tidal forcing shift.

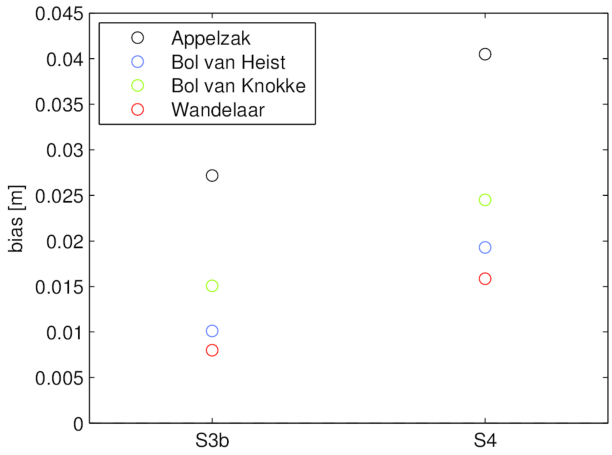

Figure 7: Bias at the measurement stations of Fig. 3 with (S4) or without (S3b) taking meteorological conditions into account.

choice since large scale tidal models that provide tidal boundary conditions are best suited for deep areas. In the second configuration, the computational domain is extended to deeper parts of the Northern Atlantic Ocean, with the aim to simulate explicitly, in a later stage of the project, the formation of storm surges and wind waves, together with their propagation toward the Belgian Continental Shelf. Both approaches lead to similar and satisfactory results in terms of tidal modelling.

Taking meteorological conditions into account do not alter the quality of the results during a calm period, and improved them significantly during a windy period. In particular, the model is able to reproduce rather satisfactorily the storm surge of December 5-6.

REFERENCES

[1] B. de Brye, A. de Brauwere, O. Gourgue, T. Kärnä, J. Lambrechts, R. Comblen, et al., A finite-element, multi-scale model of the Scheldt tributaries, river, estuary and ROFI, Coastal Engineering. 57 (2010) 850–863.

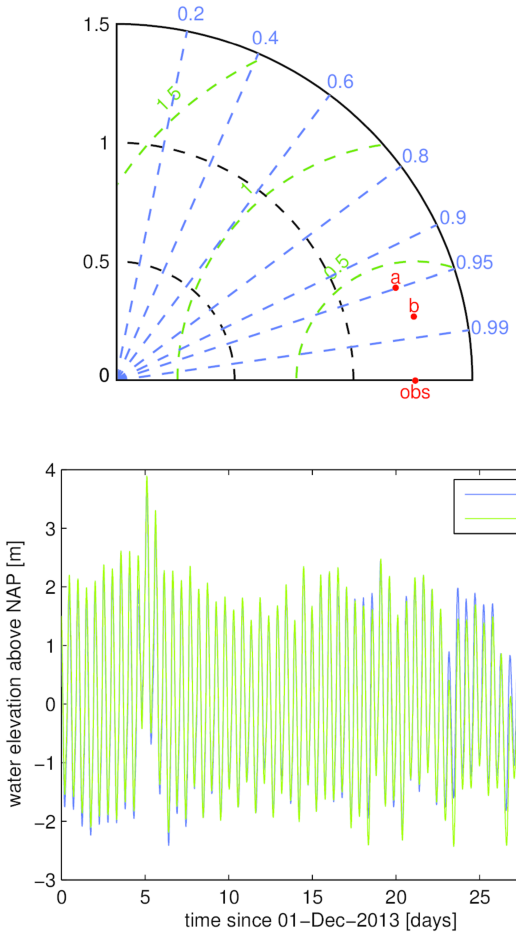

Figure 8: [Upper panel] Taylor diagram comparing water elevation from simulations S5a and S5b with observations at Wandelaar; standard deviations σ_f and σ_r are given in black, correlation coefficient R in blue, and centered pattern RMS error E' in green. [Bottom panel] Water elevation time series at Wandelaar from simulation S5b and observations.

[2] J. Lambrechts, R. Comblen, V. Legat, C. Geuzaine, J.-F. Remacle, Multiscale mesh generation on the sphere, Ocean Dynamics. 58 (2008) 461–473.

[3] C. Geuzaine, J.-F. Remacle, Gmsh: A 3-D finite element mesh generator with built-in pre- and post-processing facilities, International Journal for Numerical Methods in Engineering. 79 (2009) 1309–1331.

[4] R.A. Flather, Results from surge prediction model of the North-West European continental shelf for April, November and December 1973, United Kingdom, 1976.

[5] G.D. Egbert, A.F. Bennett, M.G.G. Foreman, TOPEX/POSEIDON tides estimated using a global inverse model, Journal of Geophysical Research. 99 (1994) 24821–24852.

[6] G.D. Egbert, S.Y. Erofeeva, Efficient inverse modeling of barotropic ocean tides, Journal of Atmospheric and Oceanic Technology. 19 (2002) 183–204.

[7] D.P. Dee, S.M. Uppala, A.J. Simmons, P. Berrisford, P. Poli, S. Kobayashi, et al., The ERA-Interim reanalysis: Configuration and performance of the data assimilation system, Quarterly Journal of the Royal Meteorological Society. 137 (2011) 553–597.

[8] T. Spencer, S.M. Brooks, B.R. Evans, J. a. Tempest, I. Möller, Southern North Sea storm surge event of 5 December 2013: Water levels, waves and coastal impacts, Earth-Science Reviews. 146 (2015) 120–145.

[9] K.E. Taylor, Summarizing multiple aspects of model performance in a single diagram, Journal of Geophysical Research. 106 (2001) 7183–7192.